Quaternary Geochronology 71 (2022) 101318

Contents lists available at ScienceDirect

Quaternary Geochronology

journal homepage: www.elsevier.com/locate/quageo

Extended-range luminescence chronologies for the Middle Pleistocene units at the Sima del Elefante archaeological site (Sierra de Atapuerca, Burgos, Spain)

Martina Demuro [a,*], Lee J. Arnold [a], Josep-María Parés [b], Arantza Aranburu [c], Rosa Huguet [d,e,f], Josep Vallverdú [d,e,f], Juan-Luis Arsuaga [g,h], José-María Bermúdez de Castro [b], Eudald Carbonell [d]

[a] School of Physical Sciences, Environment Institute, and Institute for Photonics and Advanced Sensing (IPAS), University of Adelaide, Adelaide, Australia
[b] Centro Nacional de Investigación Sobre La Evolución Humana (CENIEH), Burgos, Spain
[c] Facultad de Ciencia y Tecnología, Universidad del País Vasco, Leioa, Spain
[d] (IPHES-CERCA) Institut Català de Paleoecologia Humana i Evolució Social, Tarragona, Spain
[e] Departament D'Història i Història de L'Art, Universitat Rovira i Virgili, Tarragona, Spain
[f] Unidad Asociada al Consejo Superior de Investigaciones Científicas (CSIC), Departamento de Paleobiología, Museo Nacional de Ciencias Naturales, Madrid, Spain
[g] Centro Mixto Universidad Complutense-Instituto de Salud Carlos III de Evolución y Comportamiento Humanos, Madrid, Spain
[h] Facultad de Ciencias Geológicas, Universidad Complutense de Madrid, Madrid, Spain

ARTICLE INFO

Keywords:
Atapuerca
Sima del Elefante
Single-grain TT-OSL
Post IR-IR
Middle pleistocene

ABSTRACT

The Sima del Elefante site is located within the Sierra de Atapuerca karst system (Burgos, northern Spain), and forms part of a series of important Early, Middle and Late Pleistocene archaeological complexes that have been dated previously with luminescence techniques (Gran Dolina, Galería Complex, Sima de los Huesos, Galería de las Estatuas). This study focuses on the upper Middle Pleistocene units (TE18 and TE19) at Sima del Elefante, which contain Acheulean and transitional lithic assemblages (Mode 2/3), as well as large and small mammal fossils. Importantly, these uppermost units are associated with a sediment plug located in the cave's interior at Galería Baja, which marks the closure of a significant palaeoentrance to the Atapuerca karst system. Establishing the accumulation history of these related deposits is important for understanding both Lower Palaeolithic technological dynamics via comparisons with similar levels at other Atapuerca sites (i.e., Gran Dolina and Galería Complex), as well as past human occupation patterns and carnivore use of (and accessibility to) the caves. We present single-grain TT-OSL and multi-grain pIR-IR chronologies for the Sima del Elefante upper sequence and the Galería Baja sediment cone, as well as U-series dating results for a stalagmitic crust capping the combined clastic infill sequence. The paired luminescence ages for the upper occupation levels are in agreement with each other and reveal that the host deposits accumulated 576–481 ka for the TE18 stratified scree layers, 266–237 ka for TE19 and 206–250 ka for the Galería Baja upper cone section (weighted mean 2σ age ranges). A concordant U-series age of 202 ± 65 ka is obtained for the overlying stalagmitic crust at Galería Baja. The Sima del Elefante ages are consistent with those previously obtained using U-series and biochronology, confirming that there is an erosional unconformity and complex carbonate deposition phase associated with the upper layers of unit TE18 and that the original cave entrance likely closed by ~200 ka. Chronological correlation with other Atapuerca sites reveals potential equivalence between TE18 and unit TD8 (at Gran Dolina), and between TE19 and units GIIb–GIIIb (at Galería Complex) and, possibly, TD10.1 and TD10.2 (at Gran Dolina), though more refined dating is required to confirm the latter.

1. Introduction

The Sierra de Atapuerca archaeological complex, located in northern Spain (Fig. 1a), is an important karstic system with numerous sites containing key Early, Middle and Late Pleistocene palaeoanthropological, archaeological and faunal records. Many of these sites have been dated using luminescence dating techniques, including Gran Dolina (Arnold et al., 2015; Arnold and Demuro 2015), Sima del

* Corresponding author.
E-mail address: martina.demuro@adelaide.edu.au (M. Demuro).

https://doi.org/10.1016/j.quageo.2022.101318
Received 30 November 2021; Received in revised form 30 March 2022; Accepted 19 April 2022
Available online 29 April 2022

Elefante (Arnold et al., 2015; Arnold and Demuro 2015); Galería Complex (Demuro et al., 2014); Sima de los Huesos (Arnold et al., 2014; Demuro et al., 2019a) and Galería de las Estatuas (Demuro et al., 2019b). This study focuses on the upper levels of Sima del Elefante, one of Atapuerca's main palaeoanthropological sites that preserves a long Early – Middle Pleistocene sequence with Oldowan and Acheulean tools, as well as early (archaic) *Homo* sp. fossils in the lower levels. The upper levels of Sima del Elefante are associated with Mode 2 (Acheulean) and early Mode 3 lithic assemblages (Carbonell et al., 2008; Rosas et al., 2006). Previous topographic and fieldwork investigations also indicate that Sima del Elefante belongs to the Cueva Mayor-Cueva del Silo karst system and forms part of a palaeoentrance that provided access to its interior through the adjacent Galería Baja chamber (Arsuaga et al., 1997; Rosas et al., 2006; Ortega et al., 2013a). Continued accumulation of allochthonous sediments in the Galería Baja chamber and the upper levels of Sima del Elefante eventually resulted in the cave's closure. However, the chronology of these deposits has never been established. Resolving the timing of these events is significant for two reasons: firstly, it would place chronological constraint on the Mode 2 and early Mode 3 assemblages uncovered in the Sima del Elefante's upper levels and improve correlations with similar levels at other sites in the Sierra de Atapuerca (especially Gran Dolina and Galería Complex; Ollé et al., 2013, 2016); secondly, it would lead to a better understanding of Middle Pleistocene human occupation patterns for the numerous Sierra de Atapuerca sites, especially in relation to accessibility of different parts of the karst system, including the globally significant site of Sima de los Huesos. This latter site contains the largest Middle Pleistocene fossil assemblage (>6800 remains) for the genus *Homo* worldwide with associated nuclear DNA sequencing and cranial morphological analyses placing these fossils at the beginning of the Neandertal lineage (Arsuaga et al., 1997, 2014; Meyer et al., 2016).

The main aims of this study are to: (i) apply quartz single-grain thermally-transferred optically stimulated luminescence (TT-OSL) dating and K-feldspar post-infrared (IR) IR stimulated luminescence (pIR-IR) dating jointly to individual samples, and compare the consistency of the two datasets, (ii) provide the first detailed chronologies for the Sima del Elefante upper units (TE18–TE19), as well as the corresponding sediments located inside the cave at Galería Baja, and assess

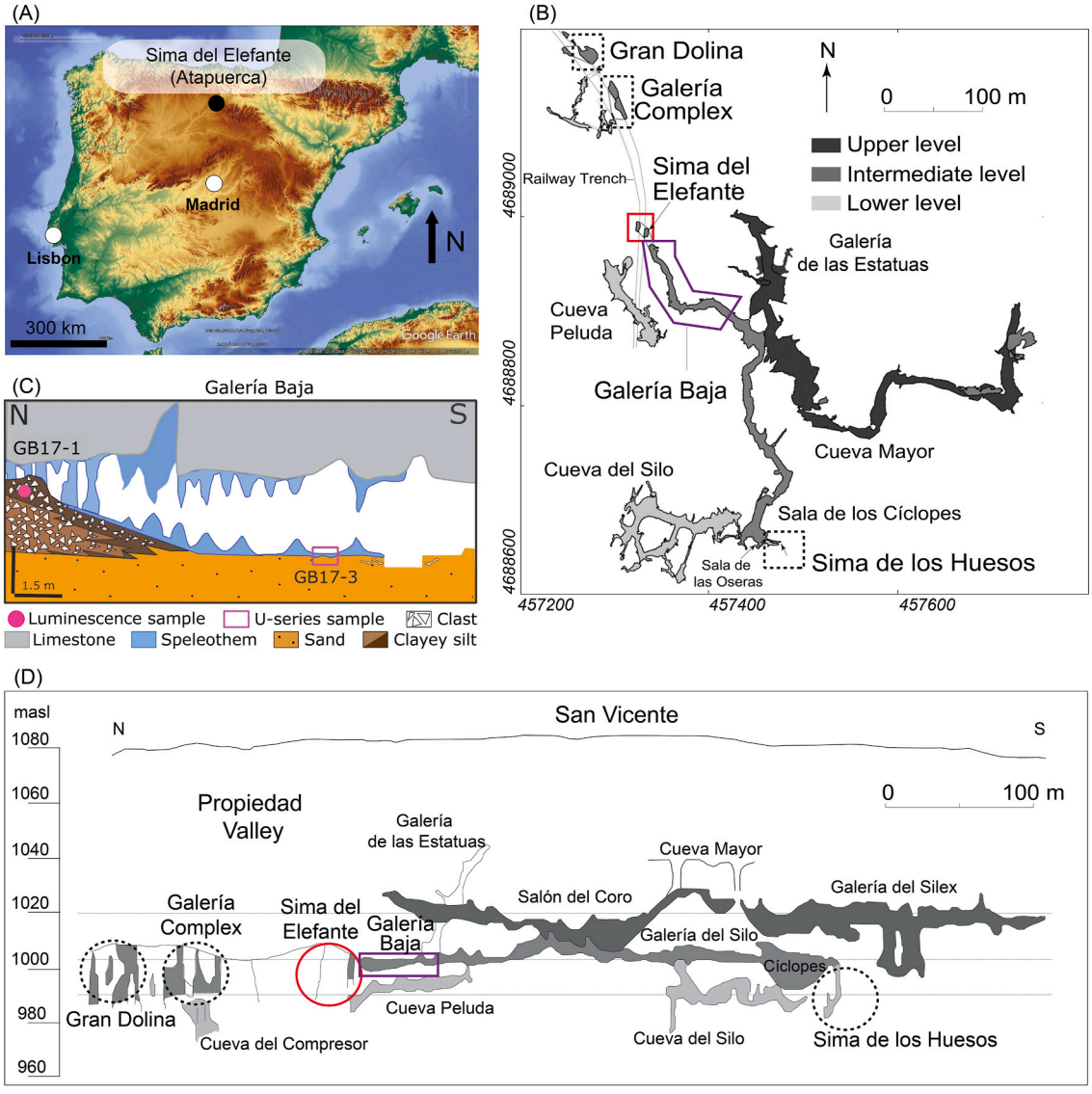

Fig. 1. (A) Map of the Iberian Peninsula showing the location of Sima del Elefante archaeological site. (B) Plan view of the endokarst system at Atapuerca (modified from Ortega et al., 2013b) showing the location of Sima del Elefante (thick red box) and Galería Baja (purple box) within the multi-level Cueva Mayor-Cueva del Silo cave system. The sites of Gran Dolina, Galería Complex and Sima de los Huesos are also shown (black dashed boxes). (C) Stratigraphy and position of dating samples (luminescence and U-series) at Galería Baja. (D) Cross-sectional view of the cave system (modified from Ortega et al., 2013b). The black dashed/red circles and purple box highlight the location of the different archaeological sites as in (B).

their temporal correlation and the timing of the cave's closure; and (iii) determine the broader chronological relationships of Atapuerca's Lower Palaeolithic (Acheulean)/early Mode 3 assemblages via comparisons with technologically similar levels at Gran Dolina (unit TD10) and Galería Complex (units GII and GIII).

2. Study sites – Sima del Elefante and Galería Baja

Sima del Elefante is situated in the intermediate level of the Cueva Mayor–Cueva del Silo multi-level karst system (42°21′00″N, 3°31′10″W; 985 masl), Sierra de Atapuerca, northern Spain, and is currently accessed through an abandoned railway trench that was excavated during the late 1800's (Fig. 1b,d) (Ortega et al., 2013b). The site is < 200 m from Gran Dolina and Galería Complex – two other significant palaeoanthropological cave sites with Lower Palaeolithic assemblages that are also situated along the railway trench – though these two neighbouring sites have not yet been directly linked to the Cueva Mayor–Cueva del Silo karst system (Ortega et al., 2013b). Sima del Elefante forms part of a now-sealed cave palaeoentrance connected to Galería Baja, a passage that is also located in the intermediate level of the karst system and leads to the interior of Cueva Mayor–Cueva del Silo (Rosas et al., 2006; Ortega et al., 2013a,b; Fig. 1b,d). According to the stratigraphic, topographic and fieldwork investigations of Rosas et al. (2006) and Ortega et al. (2013a), both the Sima del Elefante and Galería Baja cavities can be considered part of the same karstic cavity. It is hypothesised that the palaeoentrance became sealed during the Middle Pleistocene by sediments now corresponding to the upper units at Sima del Elefante and a sediment cone located at the north-west extremity of Galería Baja (Fig. 1b). At least six now-sealed palaeoentrances are reported to have been discovered for the Cueva Mayor–Cueva del Silo karst system, in addition to the two existing openings that currently provide access to the karst interior (Ortega et al., 2013a).

2.1. Sima del Elefante – stratigraphy and previous chronology

The karst sediment infill sequence at Sima del Elefante is > 25 m thick (Fig. 2a; Fig. 4) and has been subdivided into 16 lithostratigraphic units (TE7 to TE21 from the bottom upwards) (Rosas et al., 2006; Carbonell et al., 2008). Detailed descriptions of the sedimentary sequence are provided in Rosas et al. (2006) and are briefly summarised in the Supplementary Information. The lower red units (TE7–TE14) are dated to 1.13 ± 0.18 Ma (TE7) and 1.22 ± 0.16 Ma (TE9) via cosmogenic nuclides and are associated with a human mandible (*Homo* sp.), faunal fossils and Mode 1 Oldowan stone tools (Carbonell et al., 2008; Bermúdez de Castro et al., 2011; Huguet et al., 2017). The middle section, which is composed of units TE15–TE17, is sterile but a palaeomagnetic reversal has been located at the top of unit TE16/base of TE17 and has been interpreted as the Brunhes-Matuyama boundary (Parés et al., 2006), thus establishing a Brunhes Chron age (<780 ka) for the overlaying units (TE17–TE21). This chronological assignment has been confirmed via extended-range luminescence dating of quartz (single-grain TT-OSL) and K-feldspar (pIR-IR$_{225}$; as defined in Section 3.1), which produced corresponding ages of 864 ± 88 ka and 804 ± 47 ka for unit TE16 and 781 ± 63 ka and 724 ± 43 ka for unit TE17 (Arnold et al., 2015). The upper units (TE18–TE19), which are the subject of this study, are currently only constrained by U-series dating of two isolated travertine deposits located towards the top of TE18. These travertine deposits were formed within erosive spring channel complexes related to distal carbonate pond deposits formed subsequently (or coevally) in the southern sector of TE19; they therefore post-date the main stratified scree deposits of TE18, and may be more closely related to the lower TE19 deposits from a chronological perspective. The travertine samples produced (unpublished) ages of 254.7 +13.1/-11.8 ka and 307.2 +22.6/-18.9 ka for the upper TE18 deposits (de Lombera-Hermida et al., 2015).

2.1.1. Sima del Elefante – Upper levels TE18–TE19

After 7 years of systematic excavations at Sima del Elefante (ending in 2005), the upper unit (TE19) has produced ~1637 faunal remains (taxa listed in the Supplementary Information) from a 4 m^2 area (Rosas et al., 2006), while the underlying unit (TE18) has not yielded any faunal remains. Biochronological examination of these faunal associations indicates a late Middle Pleistocene age for TE19 (López-García et al., 2011; Cuenca-Bescós et al., 2016), in agreement with the U-series

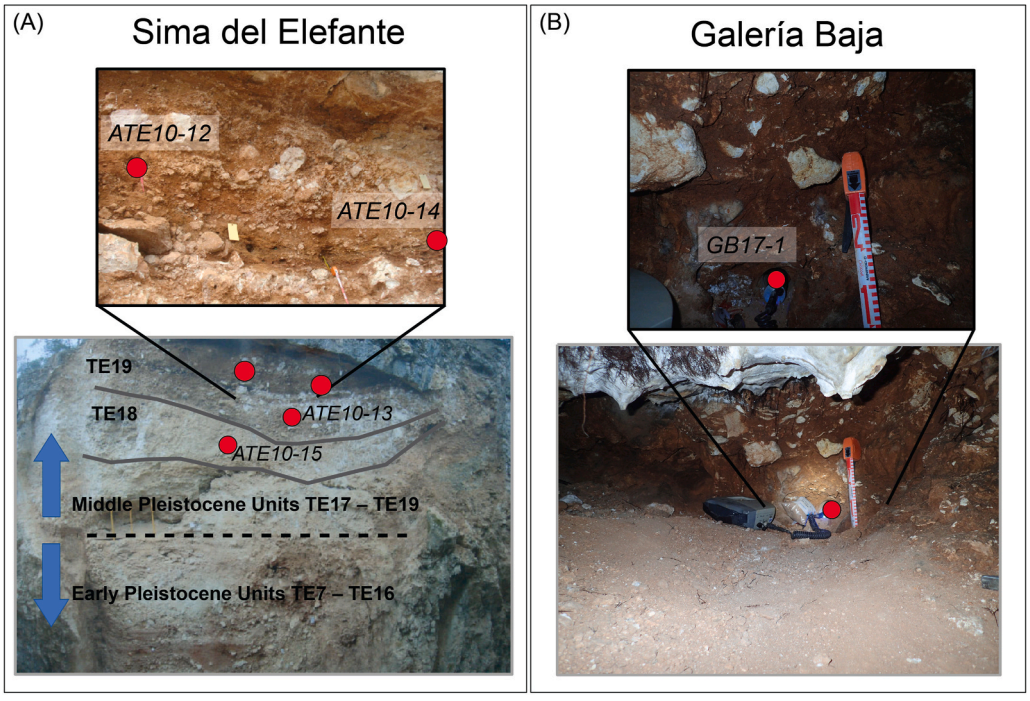

Fig. 2. (A) Photos of Sima del Elefante profile and location of the luminescence dating samples in units TE19 and TE18 (modified from Huguet et al., 2017). (B) Sampling of the sediment cone plugging the entrance at Galería Baja's north-west section.

results. Units TE18 and TE19 have produced a limited lithic assemblage of 41 pieces (mostly from TE19) that is largely made up of knapping products, flake tools and hammerstones, and a few cores (de Lombera-Hermida et al., 2015). The assemblage is composed of medium-to-large sized implements, as well as several large cutting tools (LCTs), displaying high morphological standardisation and longitudinal or centripetal reduction sequences (de Lombera-Hermida et al., 2015). Though limited in number of implements, these lithic assemblages have been classed as Mode 2 (i.e., Acheulean) in TE18 (Rosas et al., 2006) and early Mode 3 in TE19 (Rosas et al., 2006; Ollé et al., 2013; de Lombera-Hermida et al., 2015).

2.2. Galería Baja

Galería Baja is a 200 m-long karstic gallery with mean height of 1.5–3 m, which has been partially filled by Early and Middle Pleistocene sediments (Ortega et al., 2013a). These deposits are composed of three lithostratigraphic units (Fig. 1c). At the base, a sandy-siltstone unit outcrops along the entire Galería Baja chamber and contains remains of *Ursus deningeri* in the upper section (Ortega et al., 2013a); a now extinct cave bear species also found in other Middle Pleistocene sites in the Sierra de Atapuerca (García et al., 2009; Ortega et al., 2013a). These siliciclastic sediments are interpreted as fluvio-karstic deposits, probably with northward palaeocurrents. A palaeomagnetic reversal, located within this sandy-siltstone unit and below the bear remains, is interpreted as the Matuyama-Brunhes boundary. At the northern end of the Galería Baja, distal sediments of a colluvial cone formed outside the gallery were deposited above the basal unit (Ortega et al., 2013a). These external sediments, which are the subject of this study, are composed of red clays and silts with centimetre-decimetre limestone clasts. Both the colluvial and fluvio-karstic sediments are sealed by a stalagmitic crust (Fig. 1c; Ortega et al., 2013a). The existing palaeomagnetic and biochronological evidence suggests a Middle Pleistocene (or younger) age for the end of external sedimentary input in Galería Baja (Ortega et al., 2013a).

3. Methods

In total, five luminescence dating samples were collected from the Sima del Elefante upper units and the Galería Baja sediment cone. Four of these samples were obtained from the Sima del Elefante upper sequence: one (ATE10-15) from the main stratified scree deposits of unit TE18 that formed prior to the travertine deposits dated by de Lombera-Hermida et al. (2015); one (ATE10-13) from lower TE19, and two (ATE10-12 and ATE10-14) from upper unit TE19 (Fig. 2a; Fig. S1). An additional sample (GB17-1) was collected from the top of the sediment cone located at the end of the Galería Baja conduit inside Cueva Mayor (Fig. 2b). An additional calcite sample (GB17-3) was obtained from the stalagmitic crust that seals the sediment cone at Galería Baja for the purpose of U-series dating. This stalagmitic crust lies stratigraphically above luminescence dating sediment sample GB17-1 (Fig. 2b).

3.1. Luminescence dating: instrumentation, dose rate and equivalent dose (D_e) estimation

Several Risø TL/OSL-DA-20 readers with dual laser single-grain attachments, EMI 9235QB or Electron Tubes PDM 9107 B photomultiplier tubes, and spatially calibrated $^{90}Sr/^{90}Y$ β sources (~5.3–9.2 Gy/min) were used for measuring single-grain TT-OSL and multi-grain pIR-IR signals. TT-OSL measurements were made on quartz grains loaded into single-grain aluminium discs with 300 μm-deep holes. The TT-OSL signals were stimulated using a green laser (532 nm) and UV emissions were detected through a 7.5 mm-thick U-340 Hoya filter. pIR-IR signals were measured using K-feldspar-rich grain fractions that had been mounted as monolayers on stainless steel discs (~160 grains on each disc). pIR-IR signals were stimulated using an IR diode array, with blue emissions measured through a BG39 (4 mm), 7–59 (3 mm) and GG400 (3 mm) filter pack.

Environmental dose rates have been calculated using a combination of in situ gamma spectrometry and low-level beta counting (Table S1). Concentrations of K, U and Th were determined from field gamma spectra using the 'energy windows' method (Arnold et al., 2012a) and external gamma dose rates were calculated using the conversion factors of Guérin et al. (2011). The external beta dose rates were calculated from measurements made on a Risø GM-25-5 beta counter, using homogenised sediment sub-samples collected from the main luminescence dating sample positions. Cosmic-ray dose rates have been calculated using the approach described in Prescott and Hutton (1994). The beta, gamma and cosmic-ray dose rates have been corrected for long-term sediment moisture contents (Aitken, 1985), which are taken to be equivalent to 60% of saturated water content values based on proportional saturation water content assessments made on a range of freshly preserved deposits in different parts of the closed cave system (Arnold et al., 2014, 2015, Demuro et al., 2019a, b). The resultant long-term water contents of these samples ranged between 15% and 30% of dry weight, and have been assigned a relative uncertainty of 20% to accommodate any minor variations in hydrologic conditions during burial. An average K content of 12.5% ± 0.5% was assumed for calculating the internal dose rate of K-feldspar grains (Huntley and Baril, 1997). Further details of the dose rate determination procedures are provided in Table S1.

All samples were prepared using standard preparation procedures to extract purified, HF-etched 90–125 μm and 125–180 μm quartz grains, and 90–125 μm and 90–180 μm K-feldspar-rich fractions (Aitken, 1998; Murray et al., 2021; Méndez-Quintas et al., 2018). The single-aliquot regenerative-dose (SAR) protocols used to obtain equivalent dose (D_e) values are shown in Table S2. Multi-grain pIR-IR measurements were made on 90–125 μm or 90–180 μm K-feldspar grains using stimulation temperatures of 225 °C, following Buylaert et al. (2012). The suitability of this SAR procedure (herein referred to as pIR-IR_{225}) is supported by a dose-recovery test performed on sample ATE10-12 (measured to given dose ratio = 0.94 ± 0.03; see Supplementary Information), as well as similar assessments made on other sediment layers at Sima del Elefante (Arnold et al., 2015). K-feldspar pIR-IR_{225} fading rates have been determined using the published procedures of Auclair et al. (2003) and Huntley and Lamothe (2001). Single-grain TT-OSL measurements have been made using the protocol of Stevens et al. (2009), which has been modified to measure individual grains (e.g., Demuro et al., 2014) and is supported by reliable dose recovery test results (measured to given dose ratio of 0.95 ± 0.14; see Supplementary Information). The approaches used to calculate individual D_e estimates for grains/aliquots, including the SAR rejection criteria adopted in this study, are as described in previous single-grain TT-OSL and pIR-IR dating studies of Middle Pleistocene sediments from the Sierra de Atapuerca sites (see Demuro et al., 2014; Arnold et al., 2014, 2015), and are further outlined in the Supplementary Information.

3.2. U-series dating procedure

U-series dating of calcite sample GB17-3 from Galería Baja was undertaken at the Isotope Laboratory of Xi'a Jiaotong University using a multi-collector inductively coupled plasma mass spectrometer (MC-ICP-MS). Full details of the instrumentation, standardisation and calibrations used are reported in Cheng et al. (2000) and Cheng et al. (2013). Separation of U and Th isotopes for dating of the speleothem was performed following standard chemical procedures (see Edwards et al., 1987). All U–Th isotopes were measured on a Thermo-Scientific Neptune MC-ICP-MS. A triple-spike (^{229}Th–^{233}U–^{236}U) isotope dilution method was used to correct for instrumental fractionation and to determine U–Th isotopic ratios and concentrations. The procedures for characterising the electron multiplier are described in Cheng et al.

(2000). The ^{230}Th/U age and its precision (presented at 2σ) were calculated using a half-live of 75,584 ± 30 years for ^{230}Th and 245,620 ± 70 years for ^{234}U (Cheng et al., 2013). The calculated uncertainties for the U–Th isotopic data include corrections for blanks, multiplier dark noise, abundance sensitivity, and contents of the same nuclides in spike solution.

4. Results

4.1. TT-OSL and pIR-IR signal characteristics

The measured TT-OSL signals are fast-decaying and generally depleted by >90% within the first 0.18 s of stimulation. An example of a sensitivity-corrected dose-response and TT-OSL decay curve for a moderately bright grain that passed the SAR rejection criteria is shown in Fig. 3a. Between 3 and 10% of measured quartz grains per sample passed the single-grain TT-OSL SAR rejection criteria, with 60–80% producing non-detectable TT-OSL signals (Table S5). The single-grain TT-OSL dose-response curves are all well-represented by a single saturating exponential function, and display continued signal growth at high doses (10^2–10^3 Gy) (Fig. 3a). These TT-OSL signal characteristics are similar to those reported for quartz grains from the Sierra de Atapuerca Middle Pleistocene site of Galería Complex (Demuro et al., 2014).

The measured pIR-IR$_{225}$ decay curves of the Elefante and Galería Baja samples typically decrease by >90% within the first 50 s of stimulation and are optimally fitted with a single saturating exponential plus linear function. For all samples, the D_e values were obtained from the non-saturated region of the dose-response curve. Fig. 3c shows a representative pIR-IR$_{225}$ decay curve and sensitivity-corrected dose-response. The degree of athermal loss of K-feldspar pIR-IR$_{225}$ signals over burial timescales was examined through anomalous fading assessments made on subsets of aliquots for the Sima del Elefante samples (3 aliquots per sample) that had been used to derive D_e values. The mean fading rates for individual samples range between 1.40 ± 0.16 and 1.51 ± 0.18%/decade and the combined weighted average ($n = 12$) g-value is 1.44 ± 0.04%/decade. These empirical fading rates are similar to the low pIR-IR g-values reported for other Atapuerca karstic infill deposits (Demuro et al., 2014; Arnold et al., 2014). They are also consistent with published *g*-values for higher temperature pIR-IRSL signals (e.g., pIR-IRSL$_{290}$ signals; see summary in Arnold et al., 2015) and athermally stable quartz OSL signals (Buylaert et al., 2012). Previous studies have considered such low g-values (on the order of 1–2%/decade) to be potentially unreliable indicators of long-term fading rates or artefacts of laboratory procedures (see discussions in Arnold et al., 2015). As such, we have not applied an empirical fading correction to the pIR-IR ages obtained in this study; though the fading corrected ages of the Sima del Elefante samples are presented in the Supplementary Information and Table S9 for comparative purposes.

4.2. D_e distributions

Most of the single-grain TT-OSL D_e distributions display relatively

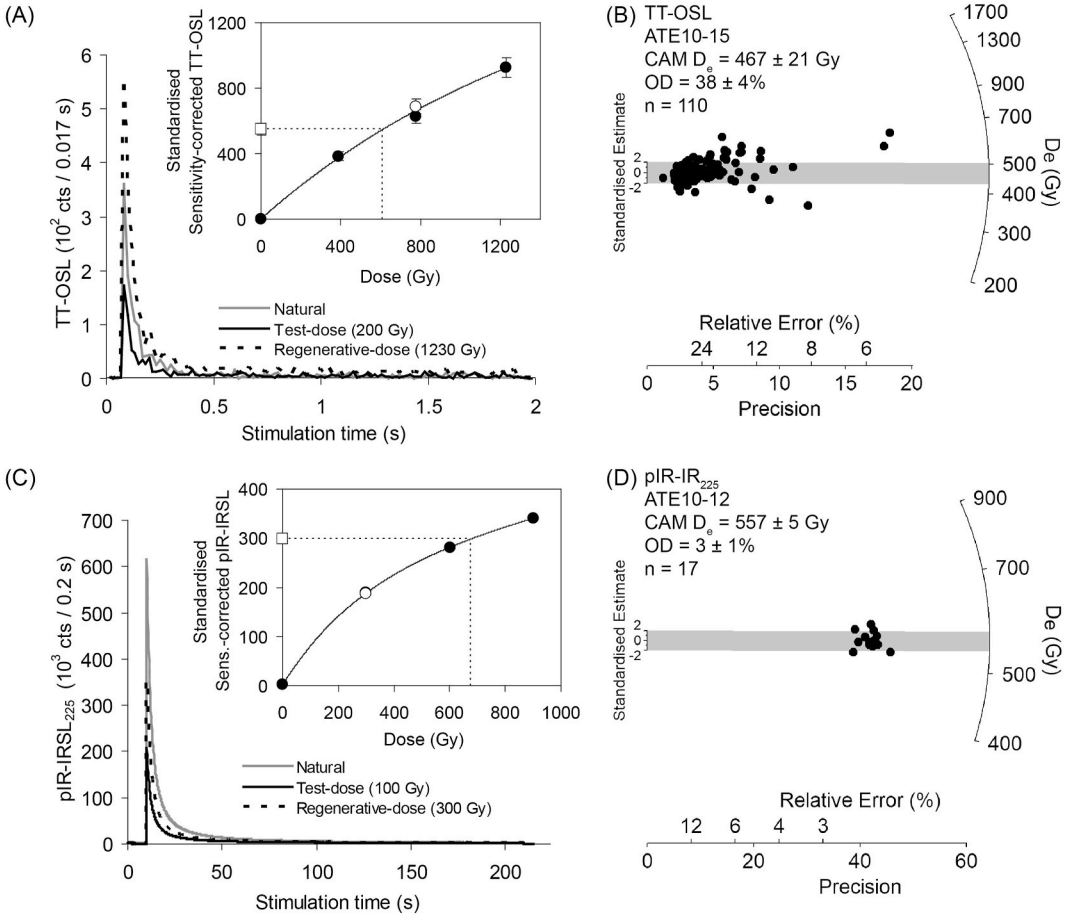

Fig. 3. Examples of (A) TT-OSL decay curves and sensitivity-corrected dose-response curve (inset) for a grain of sample ATE10-15 and (C) pIR-IR$_{225}$ decay curves and sensitivity-corrected dose-response curve (inset) for a 160-grain aliquot of sample ATE10-12. In both (A) and (C) the dose-point corresponding to the repeated regenerative-dose point (i.e., recycling ratio) is shown as a white circle and the sensitivity-corrected natural signal is shown as a white square. Radial plots show (B) the single-grain TT-OSL D_e distribution for sample ATE10-15 and (D) the multi-grain pIR-IR$_{225}$ D_e distribution for sample ATE10-12 (D_e errors are shown at 1σ). The grey band is centred on the central age model D_e obtained for each dataset.

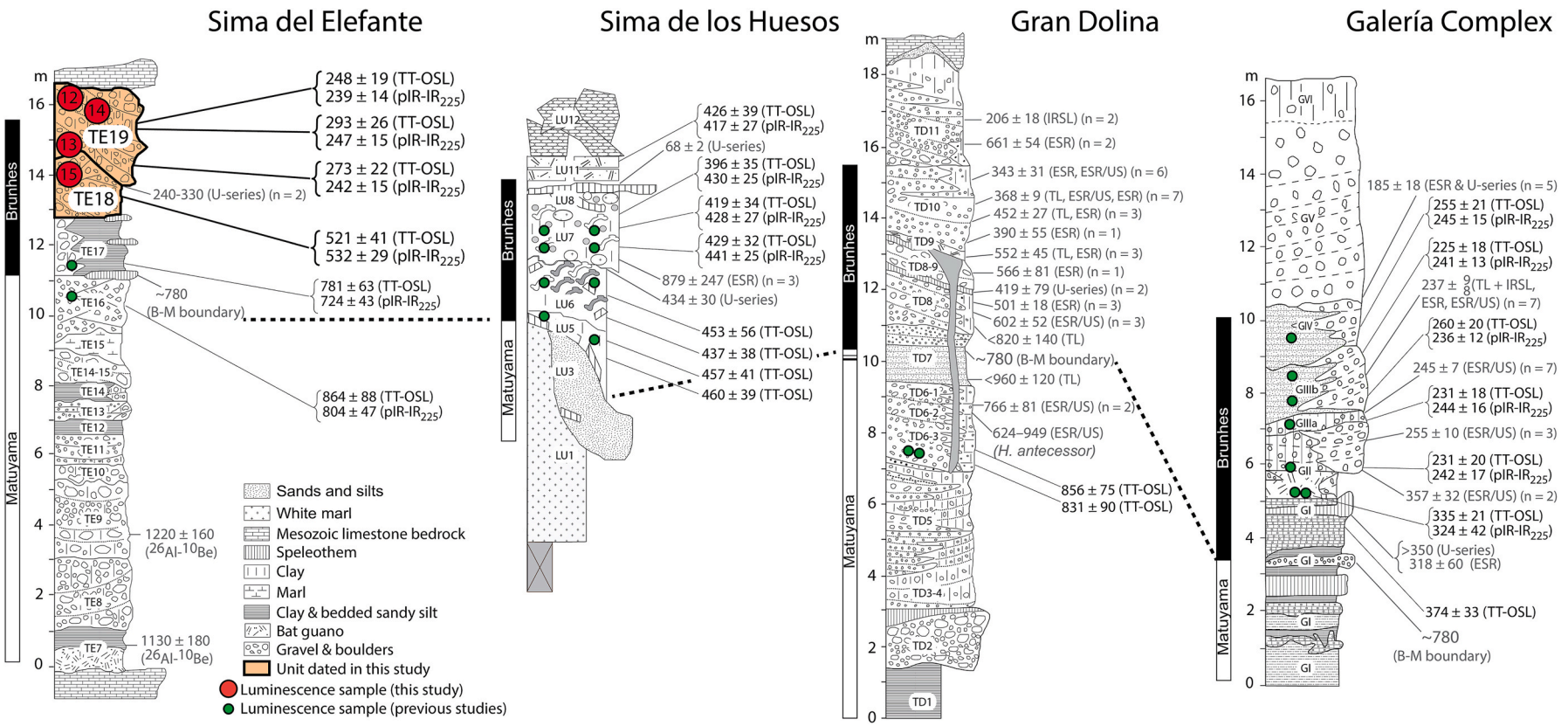

Fig. 4. Stratigraphic logs and chronologies (in thousand years = ka) for the four main Middle Pleistocene Atapuerca sequences of archaeological, palaeoanthropological and palaeontological significance: Sima del Elefante (Parés et al., 2006; Carbonell et al., 2008; Arnold et al., 2015; de Lombera-Hermida et al., 2015), Sima de los Huesos (Arsuaga et al., 2014; Arnold et al., 2014; Demuro et al., 2019a), Gran Dolina (Falguères et al., 1999; Berger et al., 2008; Parés et al., 2013; Arnold et al., 2015; Moreno et al., 2015; Duval et al., 2018), Galería Complex (Aguirre et al., 1994; Berger et al., 2008; Falguères et al., 2013; Demuro et al., 2014). ^{26}Al–^{10}Be = cosmogenic nuclide dating; ESR = electron spin resonance; US = U-series; TT-OSL = thermally-transferred optically stimulated luminescence; pIR-IR_{225} = post infrared (IR) IR; IRSL = infrared stimulated luminescence; TL = thermoluminescence; B-M boundary = Brunhes-Matuyama boundary.

low scatter (overdispersion values are 22–30%; Fig. S2), though samples ATE10–15 and GB17-1 display moderate scatter, with overdispersion values of 38% and 40%, respectively. Visual inspection of the corresponding D_e distributions for ATE10–15 and GB17-1 show that this D_e scatter is randomly spread around the mean, and is primarily attributable to a small number of precise low and high outlying D_e values (radial plots in Fig. 3b and Fig. S2e). Indeed, neither of these samples are significantly positively skewed, according to the criterion outlined by Arnold and Roberts (2009) (Table S6). Collectively, the D_e datasets of all five samples suggest that the TT-OSL signals were well bleached at deposition and not significantly affected by syn-depositional mixing complications within the karst cavities (e.g. Arnold et al., 2019). This interpretation is supported by application of the maximum log likelihood (L_{max}) score criterion of Arnold et al. (2009)(see footnote d in Table S6). In all cases, the central age model (CAM), produces the optimal model fit for D_e estimation when compared with the 3- and 4-parameter minimum age models (MAM-3 and MAM-4) of Galbraith et al. (1999). Consequently, we have used the CAM D_e values to derive representative single-grain TT-OSL burial dose estimates and final ages for the Sima del Elefante and Galería Baja samples (Table 1).

The majority of the pIR-IR_{225} D_e distributions cover a narrow range (radial plots shown in Fig. 3d and Fig. S3a-d), and, with the exception of GB17-1 (Fig. S3e) and ATE10-14 (Fig. S3b), all samples have normal distributions when assessed using the log weighted skewness test (Table S7). Similarly, the pIR-IR_{225} overdispersion values are generally low (<10% at 1σ; Table 1 and Table S7) and are consistent at 2σ with the mean value of 5 ± 1% obtained for well-bleached, unmixed samples elsewhere at Atapuerca (Demuro et al., 2014; Arnold et al., 2014). These observations suggest that, for the majority of the samples, any dose dispersion originating from extrinsic or intrinsic sources are relatively insignificant in relation to the size of the measurement uncertainties. We have used the CAM to derive the final pIR-IR_{225} burial doses estimates for the Elefante samples (also supported by the L_{max} scores obtained; Table S7). The D_e distribution of sample GB17-1 is significantly positively skewed and its overdispersion value (9 ± 2%) is slightly higher than the Elefante samples, both of which may be indicative of more significant partial bleaching or syn-depositional mixing complications (especially given the potential for multi-grain averaging effects). However, the enhanced dose dispersion for GB17-1 is primarily attributable to a single outlying D_e value, and the L_{max} test indicates that the CAM provides the optimal statistical fit for this sample when compared to the MAM-3 and MAM-4 (see L_{max} scores obtained in Table S7). In accordance with these L_{max} test results, we have opted to use the CAM to calculate the final dose estimate for GB17-1. However, it is worth emphasising that all three age models (CAM, MAM-3, MAM-4) produce statistically indistinguishable age estimates for GB17-1 at 1σ (Table S7), and therefore our interpretations are not unduly influenced by age model choice in this instance.

4.3. Luminescence and U-series ages

Table 1 summarises the final luminescence dating results obtained in this study. The paired luminescence ages of the four Sima del Elefante sediment samples are consistent both stratigraphically and between the two methods (when considering their 2σ age ranges). The consistency of the pIR-IRSL ages and replicate single-grain TT-OSL datasets provides support that an empirical fading correction is not necessary for the pIR-IR_{225} signals of these samples. The single-grain TT-OSL and multi-grain pIR-IR_{225} ages obtained for unit TE18 are 521 ± 41 ka and 532 ± 29 ka (sample ATE10-15), respectively (Table 1). The corresponding ages obtained for TE19 are significantly younger (at 2σ) and relatively uniform through the unit: 273 ± 22 ka and 242 ± 15 ka for the lower part of TE19 (sample ATE10-13), and 248 ± 19 ka and 239 ± 14 ka (sample ATE10-12) and 293 ± 26 ka and 247 ± 15 ka (sample ATE10-14) for the middle/upper part of unit TE19 (Table 1). The TT-OSL and pIR-IR_{225} ages obtained for the upper section of the sedimentary cone at Galería

Table 1
Summary of single-grain TT-OSL and multi-grain pIR-IR_{225} dating results for the Sima del Elefante and Galería Baja samples.

Sample	Unit	Single-grain TT-OSL [a]						Multi-grain pIR-IR_{225} [e]					
		Accepted/measured grains		Grain size (μm)	OD (%) [b]	D_e (Gy) [c]	Total dose rate for Qz (Gy/ka)	Age (ka) [d]	Accepted/measured aliquots	Grain size (μm)	OD (%) [b]	D_e (Gy) [c]	Total dose rate for K-feldspars (Gy/ka)	Age (ka) [d]
Sima del Elefante														
ATE10-12	TE19 (middle)	106/1100		90–125	30 ± 3	464 ± 18	1.87 ± 0.12	248 ± 19	17/17	90–125	3 ± 1	557 ± 5	2.33 ± 0.12	239 ± 14
ATE10-14	TE19 (middle)	52/1200		125–180	23 ± 5	531 ± 25	1.81 ± 0.13	293 ± 26	11/11	90–180	5 ± 1	609 ± 10	2.46 ± 0.14	247 ± 15
ATE10-13	TE19 (lower)	99/1400		125–180	23 ± 3	522 ± 18	1.92 ± 0.13	273 ± 22	12/12	90–180	6 ± 2	621 ± 12	2.56 ± 0.14	242 ± 15
ATE10-15	TE18	110/1500		90–125	38 ± 4	467 ± 21	0.90 ± 0.06	521 ± 41	11/11	90–125	5 ± 1	721 ± 12	1.36 ± 0.07	532 ± 29
Galería Baja														
GB17-1	Cone (upper)	48/1600		90–125	41 ± 6	355 ± 26	1.57 ± 0.09	226 ± 21	12/12	90–125	9 ± 2	475 ± 13	2.03 ± 0.09	234 ± 13

[a] TT-OSL measurements were made using the 'pseudo' single-grain approach (i.e., ~18 grains per hole; Arnold et al., 2012b).
[b] OD = overdispersion.
[c] D_e values have been calculated using the central age model (CAM; Galbraith et al., 1999).
[d] Mean ± total uncertainty (68% confidence interval), calculated as the quadratic sum of the random and systematic uncertainties. Total uncertainty includes a systematic component of ±2% associated with laboratory beta-source calibration.
[e] pIR-$IRSL_{225}$ measurements were made using 160-grain aliquots.

Table 2
U-series dating results for sample GB17-3 (Fig. 1c) collected from the stalagmitic crust capping external sediments at Galería Baja. Age uncertainties are reported at 2σ.

Sample number	^{238}U (ppb)	^{232}Th (ppt)	^{230}Th/^{232}Th (atomic × 10^6)	δ^{234}U* (measured)	^{230}Th/^{238}U (activity)	^{230}Th Age (yr) (uncorrected)	^{230}Th Age (yr) (corrected)	$\delta^{234}U_{initial}$** (corrected)	^{230}Th Age (yr B.P.)*** (corrected)
GB17-3	87.1 ± 0.2	193,732 ± 3,900	7.89 ± 0.17	123.0 ± 4.8	1.0649 ± 0.0067	273,342 ± 9,315	202,194 ± 65,002	218 ± 40	202,125 ± 65,002

U decay constants: $\lambda_{238} = 1.55125 \times 10^{-10}$ a^{-1} (Jaffey et al., 1971) and $\lambda_{234} = 2.82206 \times 10^{-6}$ a^{-1} (Cheng et al., 2013). Th decay constant: $\lambda_{230} = 9.1705 \times 10^{-6}$ a^{-1} (Cheng et al., 2013).
*$\delta^{234}U = [(^{234}U/^{238}U]_{activity} - 1) \times 1000$. **$\delta^{234}U_{initial}$ was calculated based on ^{230}Th age (T), i.e., $\delta^{234}U_{initial} = \delta^{234}U_{measured} \times e^{\lambda 234 \times T}$. ***B.P. stands for "Before Present" where the "Present" is defined as the year 1950 A.D.
Corrected ^{230}Th age assumes the initial ^{230}Th/^{232}Th atomic ratio of 4.4 (±2.2) × 10^{-6}. i.e., the values for a material at secular equilibrium, with the bulk earth ^{232}Th/^{238}U value of 3.8. The errors on these values are arbitrarily assumed to be 50%.

Baja are 226 ± 21 ka and 234 ± 13 ka (sample GB17-1), respectively, which are indistinguishable from each other at 1σ.

The U-series dating results for sample GB17-3 are shown in Table 2. The calcite fragment has a ^{238}U content of 87.1 ± 0.2 ppb, which is similar to values obtained for other speleothem samples from the Cueva Mayor–Cueva del Silo karst system (e.g., Bischoff et al., 2003; Martínez-Pillado et al., 2014), as well as a relatively high ^{232}Th content of 193,732 ± 3900 ppt and a low ^{230}Th/^{232}Th ratio of 7.89 ± 0.17. As the latter ratio is indicative of some detrital particles in the calcium carbonate matrix, the final U-series age has been calculated after including a detrital correction. The corrected ^{230}Th/U age assumes an initial ^{230}Th/^{232}Th atomic ratio of 4.4 (±2.2) × 10^{-6}, which is the value for material at secular equilibrium with a bulk earth ^{232}Th/^{238}U value of 3.8. Using this approach, a corrected U-series age of 202 ± 65 ka (2σ) is obtained for the stalagmitic crust sealing the sediment deposition at Galería Baja (sample GB17-3; Fig. 1c), in good agreement with the underlying luminescence ages (Tables 1 and 2).

5. Discussion and conclusion

The new luminescence ages obtained for the Sima del Elefante upper units reveal that TE18 and TE19 were deposited 576–481 ka ($n = 2$) and 266–237 ka ($n = 6$), respectively (2σ age range of weighted mean from all combined TT-OSL and pIR-IR$_{225}$ ages for each unit, as shown in Table 1). These ages are in agreement with the independent age control available for the underlying units TE16 and TE17, which collectively record the Brunhes–Matuyama palaeomagnetic reversal (Parés et al., 2006) and have corresponding TT-OSL and pIR-IR$_{225}$ ages of 804 ± 47 ka and 864 ± 88 ka (TE16), and 781 ± 63 ka and 724 ± 43 ka (overlying unit TE17) (Arnold et al., 2015). Importantly, the new luminescence ages for the stratified scree layers of TE18 and TE19 are in good agreement with (i.e., bracket) the two intervening U-series ages of 254.7 +13.1/-11.8 ka and 307.2 +22.6/-18.9 ka obtained for localised travertines found towards the top of unit TE18 (de Lombera-Hermida et al., 2015) (Fig. 4). These results indicate that deposition of the upper Sima del Elefante section spanned marine isotope stage (MIS) 15 through to MIS 7 (Lisiecki and Raymo, 2005). They also confirm that the erosive channel travertine deposits found in the southern sector of TE18 post-date the underlying stratified scree TE18 deposits by at least 151 ka, and they are more closely related (at least chronologically) to the lower TE19 deposits or the unconformity between units TE18 and TE19. Deposition of the TE18 stratified scree layers likely occurred during MIS 15–13, with subsequent erosion and travertine carbonate re-deposition occurring significantly later during MIS 9. The beginning of sediment deposition for unit TE19 similarly occurred significantly later, during MIS 9 at the earliest (oldest possible age at 2σ); though it is most likely that deposition of this unit took place largely during MIS 8–7.

The single-grain TT-OSL and multi-grain pIR-IR$_{225}$ ages of 226 ± 21 ka and 234 ± 13 ka obtained for the Galería Baja sample (GB17-1) (combined weighted mean age of 232 ± 11 ka; Table 1), show that final allochthonous sediment accumulation of this conduit occurred during MIS 7. The consistency of the ages obtained for samples GB17-1, ATE10-12 and ATE10-14 provide an additional line of evidence supporting the correlation between unit TE19 at Sima del Elefante and the sediment cone directly adjacent at Galería Baja, as suggested by Rosas et al. (2006) and Ortega et al. (2013a,b). These luminescence ages are also in close agreement with the U-series age of 202 ± 65 ka obtained for the stalagmitic crust atop the sediment cone at Galería Baja, which further confirms the MIS 7 age for these deposits.

In assessing the reliability of the extended-range chronologies obtained in this study, it is worth considering the potential for age underestimation related to anomalous fading of the pIR-IR$_{225}$ K-feldspar signals (Huntley and Lamothe, 2001), as well as thermal instability of TT-OSL quartz signals over extended burial periods (Adamiec et al., 2010). As noted earlier, we consider that an empirical fading correction is not necessary for the pIR-IR$_{225}$ signals of these samples owing to the low g-values obtained in this study – which are in agreement with those published for athermally stable quartz OSL and K-feldspar pIR-IR$_{290}$ signals (Arnold et al., 2015) – the consistency of the replicate pIR-IR and TT-OSL ages for each sample and the agreement between the (uncorrected) K-feldspar ages and the U-series ages for both the Galería Baja capping speleothem and TE18 travertine deposits. However, for comparative purposes, the fading corrected ages for the Sima del Elefante samples are summarised in Table S9. Application of the Kars et al. (2008) fading correction results in significantly older pIR-IR$_{225}$ ages, ranging between ~410 and ~480 ka for unit TE19 (samples ATE10-12, ATE10-13 and ATE10-14); a finite corrected age could not be derived for ATE10-15 from TE18 due to natural signal 'oversaturation' (see Supplementary Information for details). These fading-corrected pIR-IR ages are stratigraphically inconsistent with the underlying TE18 U-series age and do not overlap with the paired TT-OSL ages. The independent and semi-independent dating evidence therefore does not support application of an additional fading correction for these sample; a finding that is consistent with the results of related pIR-IR$_{225}$ independent age comparisons undertaken lower down in the Sima del Elefante profile (Brunhes-Matuyama boundary comparison), as well as at other Atapuerca sites (Arnold et al., 2015; Demuro et al., 2014, Arsuaga et al., 2014, Fig. 4).

The suitability of applying the Kars et al. (2008) fading correction to these samples may be further complicated for several reasons. As noted by the original authors, the applicability of this correction procedure over high dose ranges is strongly dependent on (i) the reliability of the ρ' parameter estimate – which may be incorrect if, as noted earlier, our empirical g-values are partly or wholly artefacts of laboratory measurement procedures (see Buylaert et al., 2012; Arnold et al., 2015), and (ii) adequate dose response curve fitting and characterisation – which in this instance is complicated by the dose-response curves not being measured over ranges that fully constrain I_{max} dose saturation, and the fact that the original dose response curves are optimally fitted with a function that differs from that used in the Kars et al. (2008) fading model (i.e., a single saturating exponential function in the latter compared to a saturating exponential plus linear function for our empirical datasets). These potential suitability issues are borne out by the inability to derive a finite, fading-corrected D_e value via dose-response curve interpolation for one-third of the measured aliquots (Table S9).

There have been some discussions in the literature regarding TT-OSL

signal stability over Middle and Early Pleistocene timescales (Adamiec et al., 2010; Bartz et al., 2019), though reported lifetime estimates are highly variable, have large associated uncertainties, and the potential for inter-sample differences remains unclear. For the geological province under consideration here, the reliability of single-grain TT-OSL signals has been examined using a range of known-age luminescence dating studies at different Atapuerca sites (see Arnold et al., 2015). Importantly, the single-grain TT-OSL characterisation study of Arnold and Demuro (2015) highlighted three important findings with regards to thermal stability at these sites: (i) thermal stability inferences made using multi-grain TT-OSL signals (e.g., Adamiec et al., 2010) cannot simply be extrapolated to single-grain TT-OSL measurements due to averaging effects, the significant influence of non-TT-OSL-producing grains on composite multi-grain signals, as well as interference from grains with slowly bleaching OSL components (i.e., carry over from OSL decays rather than genuine TT-OSL signals); (ii) there can be significant variability in TT-OSL signal stability characteristics for a given sample at the single-grain level, further questioning the representativeness of single value, multi-grain lifetime assessments. Indeed, independent age comparisons undertaken at a range of Early and Middle Pleistocene sites in the region confirm that it is possible to obtain reliable single-grain TT-OSL ages over timescales that exceed existing multi-grain TT-OSL lifetime estimates (e.g., Arnold et al., 2015; Bartz et al., 2019; Demuro et al., 2015, 2020; Duval et al., 2020, this volume); and (iii) where samples have been adversely affected by TT-OSL thermal stability issues, this is clearly distinguishable at the single-grain level by the presence of high overdispersion and discrete low dose components. In the present study we do not observe any such complex, multi-modal D_e distributions that would otherwise by indicative of thermally unstable grain populations.

Regardless of the debate surrounding the long-term stability of the TTOSL signal, the potential implications for our single-grain TT-OSL ages appear to be relatively unimportant given the burial temperatures and timescales of relevance to this study. If, for example, we consider the mean annual ambient temperature inside the Cueva Mayor system (10.8 °C; Atapuerca meteorological station, Spain; Martín-Chivelet et al., 2011) and assume that the laboratory lifetime measurements of Adamiec et al. (2010) are directly applicable to our samples, the expected TT-OSL ages would only change by 7–30 kyr according to the fractional loss equation of Aitken (1985) (i.e., the ages do not change beyond their existing errors). Long-term mean ambient temperatures inside the cave system would need to have been consistently in excess of 20 °C for the corrected TT-OSL ages to be in agreement with the fading corrected K-feldspar ages shown inTable S9 (assuming that both the uncorrected K-feldspar and existing TT-OSL ages are genuinely affected by stability issues). Such temperature shifts are not realistic in the closed karst system, and are even less realistic when considering that the long-term burial periods of these samples span several glacial stages, which were characterised by significantly reduced ambient temperatures.

Further examination of the TT-OSL and pIR-IR_{225} stability characteristics of these particular samples would be worthwhile in future studies. However, the consistency of the replicate luminescence datasets, their agreement with stratigraphically related U-series chronologies, and broader agreement with independent and semi-independent age control at several other Atapuerca sites (Demuro et al., 2014; Arsuaga et al., 2014; Arnold et al., 2015; Duval et al., 2022), would be unlikely if either or both signals were independently affected by different types of stability complications. Based on the available empirical evidence, we therefore consider the uncorrected pIR-$IRSL_{225}$ and TT-OSL ages suitable for interpretation of the TE18-19 and Galería Baja archaeo-stratigraphic sequences.

The new luminescence and U-series dating results provide the first reliable chronological constraint on the closure of the Sima del Elefante/Galería Baja palaeoentrance. Our results reveal that this event occurred during MIS 7 and the process was likely fully completed by ~200 ka. This age is in agreement with the presence of *Ursus deningeri* remains attached to the dated stalagmitic crust at Galería Baja. This bear species has an age range that extends well into the Middle Pleistocene but was replaced by *Ursus spelaeus* in the Late Pleistocene (García et al., 1997; Pacher and Stuart, 2009). Remains of *Ursus deningeri* are abundant at the site of Sima de los Huesos, as well as in the test trenches located in the adjacent chambers of Sala de los Cíclopes and Sala de las Oseras (both located on the southern side of the intermediate section of the karst system (Fig. 1b); García et al., 1997). It is feasible that these Middle Pleistocene bear populations entered the cave through the Sima del Elefante/Galería Baja palaeoentrance and made their way into Sima de los Huesos (500 m away) through the interconnected galleries. This interpretation is supported by the preservation of bear beds throughout the passageways between Sima del Elefante/Galería Baja and Sima de los Huesos, indicating that the former was the likely point of entry. The closing of the Sima del Elefante/Galería Baja palaeoentrance by ~200 ka is compatible with the exclusive presence of the Middle Pleistocene bear species (*Ursus deningeri*) in the deeper sectors of the Cueva Mayor–Cueva del Silo system. In contrast, there are no remains of the Late Pleistocene bear species *Ursus spelaeus* in the Sima de los Huesos/Sala de los Cíclopes chambers (Arsuaga et al., 1997), indicating that the original access point had already been closed by the end of the Middle Pleistocene. Our MIS 7 ages for the uppermost Sima del Elefante and Galería Baja infill sediments confirm this interpretation and suggest that the closure of the Sima del Elefante/Galería Baja entrance may have played a major role in the bear occupation dynamics of the Cueva Mayor–Cueva del Silo system. The intriguing question of how Middle Pleistocene human populations accessed the deeper parts of the Cueva Mayor system remains less well resolved. If humans were accessing the deeper karst cavities via Sima del Elefante/Galería Baja prior to 200 ka then they would certainly have needed burning torches to aid navigation.

Our new ages for Sima del Elefante also provide scope to re-examine the broader chronological relationships of Atapuerca's Lower Palaeolithic (Acheulean) and early Middle Palaeolithic assemblages. Fig. 4 shows the four main Early/Middle Pleistocene sequences at Atapuerca that have been systematically excavated (Sima del Elefante, Sima de los Huesos, Gran Dolina and Galería Complex). For each site we summarise the stratigraphic logs, together with the chronologies obtained over the past decades using extended-range luminescence dating techniques (shown in black), as well as other methods (shown in grey). It is interesting to note that between ~481 ka and ~266 ka the entrance at Sima del Elefante would have been accessible (timing between the end of deposition of TE18 and beginning of TE19 according to the 2σ of mean ages) and would have likely provided access to the karst system for humans and animals during this time. This period of opening coincides well with the timing of deposition for the red clay units (LU5 and LU6) and the overlying café con leche bone breccia (LU7) at Sima de los Huesos, as well as hominin and carnivore remains therein – The combined LU5–LU7 sequence at Sima de los Huesos has been dated to between ~450 ka and ~427 ka using the same extended-range luminescence dating methods employed here (Arnold et al., 2014; Arsuaga et al., 2014; Demuro et al., 2019a). Thus our latest results confirm that the Sima del Elefante entrance was open when the main Sima de los Huesos sediment sequence (and hominin fossils) accumulated (Fig. 4).

When comparing the dating results obtained for the upper Sima del Elefante units to the chronologies available for Gran Dolina and Galería Complex (all three sites are located in the abandoned railway trench; Fig. 1b), it can be observed that the timing of unit TE18 likely correlates with the deposition of Gran Dolina unit TD8 (650–500 ka; Fig. 4), which would be in agreement with assessments of sedimentary microfacies and soil micromorphology for both units (see Vallverdú i Poch, 2017), and possibly TD9. Gran Dolina unit TD8 largely appears to be archaeologically sterile (no material has been published yet from this unit) and the oldest Middle Pleistocene lithic reported for this site originate from unit TD9 (Ollé et al., 2013), which has an existing age of 552 ± 45 ka

(weighted mean; $n = 3$) from polymineral thermoluminescence (TL) dating of sediments and ESR dating of optically bleached grains (Berger et al., 2008; Moreno et al., 2015, Fig. 4). The single cleaver-like tool recovered from Sima del Elefante unit TE18 has been tentatively classed as Mode 2/Acheulean (Rosas et al., 2006; de Lombera-Hermida et al., 2015), and may represent one of the oldest (i.e., 481–576 ka) examples of this type of stone tool yet discovered in the Sierra de Atapuerca.

Sima del Elefante unit TE19 (266–237 ka; 2σ of weighted mean age; $n = 6$) is chronologically correlative with units GIIb–GIIIb (248–231 ka; 2σ of weighted mean age; $n = 25$) of Galería Complex (Fig. 4), which have been dated using ESR/U-series of large mammal teeth (Falguères et al., 2013), multi-grain pIR-IR_{225} and single-grain TT-OSL of sediments (Demuro et al., 2014), as well as polymineral IRSL and TL dating of sediments (selected ages from Berger et al., 2008). The lithic assemblage of TE19 comprises 36 implements (de Lombera-Hermida et al., 2015), and is largely composed of flake tools and fragments classed as transitional Mode 2 to 3. Similar assessments have been made for the lithic assemblages recovered from upper part of unit GIII at Galería Complex, as well as units TD10.1 and, possibly, TD10.2 at Gran Dolina (Ollé et al., 2013, 2016; Mosquera et al., 2013; García-Medrano et al., 2015). Both TE19 and TE18 at Elefante are older than unit TD11 at Gran Dolina, dated to ~206 ka by IRSL dating (Fig. 4; Berger et al., 2008). However, firm chronological correlation between Sima del Elefante TE19 and the Gran Dolina upper TD10 units (TD10.1 = 405–281 ka, $n = 6$ and TD10.2 = 386–350 ka, $n = 7$) is difficult to ascertain because the latter have only been dated using optically bleached quartz ESR Al-centre signals (Moreno et al., 2015), which have been shown to produce age overestimates in some Atapuerca samples (e.g., Arsuaga et al., 2014). In the absence of ESR Multiple Centre (Al versus Ti–Li versus Ti–H) assessments for these samples, Duval et al. (2018) caution that the existing Al-centre ages for Gran Dolina TD10 should be considered as maximum estimates of the true depositional ages. The use of extended-range luminescence dating at Gran Dolina is currently limited to the Early Pleistocene unit TD6 (Fig. 4). Additional pIR-IR and single-grain TT-OSL dating is now required to refine the age of the Middle Pleistocene units (TD8–TD10) at Gran Dolina and ascertain firmer chronological correlations with the Sima del Elefante and Galería Complex units that host comparable archaeological records.

Declaration of competing interest

The authors declare that they have no known competing financial interests or personal relationships that could have appeared to influence the work reported in this paper.

Acknowledgments

M.D. was supported by Australian Research Council (ARC) Future Fellowship FT200100816 and ARC Discovery Early Career Researcher Award DE160100743. J-M.P received support from grant CGL 2017-89603-R. This research was funded by the Spanish Ministry of Science, Innovation and Universities grants PGC 2018-093925-B-C31, C32, and C33. This research was conducted as part of the AGUAR project number SGR 2017–1040, the Universitat Rovira i Virgili (2014, 2015, and 2016 PFD-URV-B2-147) and CERCA Programme/Generalitat de Catalunya. We are thankful for the support from the Consejería de Cultura de la Junta de Castilla y León and the Fundación Atapuerca. We are grateful to the U-series Chronology Dating Laboratory of the Institute of Global Environmental Change, Xi'an Jiaotong University, for processing the speleothem sample. We thank Raquel Pérez-Martínez (TAUP) for her assistance in positioning the luminescence dating samples.

Appendix A. Supplementary data

Supplementary data to this article can be found online at https://doi.org/10.1016/j.quageo.2022.101318.

References

Adamiec, G., Duller, G.A.T., Roberts, H.M., Wintle, A.G., 2010. Improving the TT-OSL SAR protocol through source trap characterisation. Radiat. Meas. 45, 768–777.
Aguirre, E., 1994. Dating the Ibeas humans: attempts and question marks. Cour. Forschungsinst. Senckenberg 171, 197–204.
Aitken, M.J., 1985. Thermoluminescence Dating. Academic Press, London, p. 359.
Aitken, M., 1998. An Introduction to Optical Dating: the Dating of Quaternary Sediments by the Use of Photon-Stimulated Luminescence. Oxford University Press, Oxford, p. 267.
Arnold, L.J., Roberts, R.G., 2009. Stochastic modelling of multi-grain equivalent dose (D_e) distributions: implications for OSL dating of sediment mixtures. Quat. Geochronol. 4, 204–230.
Arnold, L.J., Demuro, M., 2015. Insights into TT-OSL signal stability from single-grain analyses of known-age deposits at Atapuerca, Spain. Quat. Geochronol. 30B, 472–478.
Arnold, L.J., Roberts, R.G., Galbraith, R.F., DeLong, S.B., 2009. A revised burial dose estimation procedure for optical dating of young and modern-age sediments. Quat. Geochronol. 4, 306–325.
Arnold, L.J., Duval, M., Falguères, C., Bahain, J.-J., Demuro, M., 2012a. Portable gamma spectrometry with cerium-doped lanthanum bromide scintillators: suitability assessments for luminescence and electron spin dating applications. Radiat. Meas. 47, 6–18.
Arnold, L.J., Demuro, M., Navazo Ruiz, M., 2012b. Empirical insights into multi-grain averaging effects from 'pseudo' single-grain OSL measurements. Radiat. Meas. 47, 652–658.
Arnold, L.J., Demuro, M., Parés, J.M., Arsuaga, J.L., Aranburu, A., Bermúdez de Castro, J.M., Carbonell, E., 2014. Luminescence dating and palaeomagnetic age constraint on hominins from Sima de los Huesos, Atapuerca, Spain. J. Hum. Evol. 67, 85–107.
Arnold, L.J., Demuro, M., Parés, J.M., Pérez-González, A., Arsuaga, J.L., Bermúdez de Castro, J.M., Carbonell, E., 2015. Evaluating the suitability of extended-range luminescence dating techniques over Early and Middle Pleistocene timescales: published datasets and case studies from Atapuerca, Spain. Quat. Int. 389, 167–190.
Arnold, L.J., Demuro, M., Spooner, N.A., Prideaux, G.J., McDowell, M.C., Camens, A.B., Reed, E.H., Parés, J.M., Arsuaga, J.L., Bermúdez de Castro, J.M., Carbonell, E., 2019. Single-grain TT-OSL bleaching characteristics: insights from modern analogues and OSL dating comparisons. Quat. Geochronol. 49, 45–51.
Arsuaga, J.L., Martínez, I., Gracia, A., Carretero, L.M., Lorenzo, C., García, N., 1997. Sima de los Huesos (Sierra de Atapuerca, Spain). The site. J. Hum. Evol. 33, 109–127.
Arsuaga, J.L., Martínez, I., Arnold, L.J., Aranburu, A., Gracia-Téllez, A., Sharp, W.D., Quam, R.M., Falguères, C., Pantoja-Pérez, A., Bischoff, J., Poza-Rey, E., Parés, J.M., Carretero, J.M., Demuro, M., Lorenzo, C., Sala, N., Martinón-Torres, M., García, N., Alcázar de Velasco, A., Cuenca-Bescós, G., Gómez-Olivencia, A., Moreno, D., Pablos, A., Shen, C.-C., Rodríguez, L., Ortega, A.I., García, R., Bonmatí, A., Bermúdez de Castro, J.M., Carbonell, E., 2014. Neandertal roots: cranial and chronological evidence from Sima de los Huesos. Science 344, 1358–1363.
Auclair, M., Lamothe, M., Huot, S., 2003. Measurement of anomalous fading for feldspar IRSL using SAR. Radiat. Meas. 37, 487–492.
Bartz, M., Arnold, L.J., Demuro, M., Duval, M., King, G.E., Rixhon, G., Álvarez Posada, C., Parés, J.M., Brückner, H., 2019. Single-grain TT-OSL dating results confirm an Early Pleistocene age for the lower Moulouya River deposits (NE Morocco). Quat. Geochronol. 49, 138–145.
Berger, G.W., Pérez-González, A., Carbonell, E., Arsuaga, J.L., Bermúdez de Castro, J.M., Ku, T.L., 2008. Luminescence chronology of cave sediments at the Atapuerca palaeoanthropological site, Spain. J. Hum. Evol. 55, 300–311.
Bermúdez de Castro, J.M., Martinón-Torres, M., Gómez-Robles, A., Prado-Simón, L., Sarmiento, S., Martín-Francés, L., Olejniczak, A., Carbonell, E., 2011. Early Pleistocene human mandible from Sima del Elefante (TE) cave site in Sierra de Atapuerca (Spain): a comparative morphological study. J. Hum. Evol. 61, 12–25.
Bischoff, J.L., Shamp, D.D., Aramburu, A., Arsuaga, J.L., Carbonell, E., Bermúdez de Castro, J.M., 2003. The Sima de los Huesos Hominids Date to Beyond U/Th Equilibrium (>350 kyr) and Perhaps to 400–500 kyr: new Radiometric Dates. J. Archaeol. Sci. 30, 275–280.
Buylaert, J.-P., Jain, M., Murray, A.S., Thomsen, K.J., Thiel, C., Sohbati, R., 2012. A robust feldspar luminescence dating method for Middle and Late Pleistocene sediments. Boreas 41, 435–451.
Carbonell, E., Bermúdez de Castro, J.M., Parés, J.M., Pérez-González, A., Ollé, A., Mosquera, M., Cuenca-Bescós, G., García, N., Granger, D.E., Huguet, R., van der Made, J., Martinón-Torres, M., Rodríguez, X.P., Rosas, A., Sala, R., Stock, G.M., Vallverdu, J., Vergés, J.M., Allué, E., Benito, A., Burjachs, F., Cáceres, I., Canals, A., Díez, J.C., Lozano, M., Mateos, A., Navazo, M., Rodríguez, J., Rosell, J., Arsuaga, J. L., 2008. The first hominin of Europe. Nature 452, 465–469.
Cheng, H., Edwards, R.L., Hoff, J., Gallup, C.D., Richards, D.A., Asmerom, Y., 2000. The halflives of U-234 and Th-230. Chem. Geol. 169, 17–33.
Cheng, H., Edwards, L.R., Shen, C.-C., Polyak, V.J., Asmerom, Y., Woodhead, J., Hellstrom, J., Wang, Y., Kong, X., Spötl, C., Wang, X., Alexander JrE, Calvin, 2013. Improvements in ^{230}Th dating, ^{230}Th and ^{234}U half-life values, and U–Th isotopic measurements by multi-collector inductively coupled plasma mass spectrometry. Earth Planet Sci. Lett. 371–372, 82–91.
Cuenca-Bescós, G., Blain, H.-A., Rofes, J., López-García, J.M., Lozano-Fernández, I., Galán, J., Núñez-Lahuerta, C., 2016. Updated Atapuerca biostratigraphy: small-mammal distribution and its implications for the biochronology of the Quaternary in Spain. Comptes Rendus Palevol 15, 621–634.

de Lombera-Hermida, A., Bargalló, A., Terradillos-Bernal, M., Huguet, R., Vallverdú, J., García-Antón, M.-D., Mosquera, M., Ollé, A., Sala, R., Carbonell, E., Rodríguez-Álvarez, X.-P., 2015. The lithic industry of Sima del Elefante (Atapuerca, Burgos, Spain) in the context of Early and Middle Pleistocene technology in Europe. J. Hum. Evol. 82, 95–106.

Demuro, M., Arnold, L.J., Parés, J.M., Pérez-González, A., Ortega, A.I., Arsuaga, J.L., Bermúdez de Castro, J.M., Carbonell, E., 2014. New luminescence ages for the Galería Complex archaeological site: resolving chronological uncertainties on the Acheulean record of the Sierra de Atapuerca, northern Spain. PLoS One 9, e110169.

Demuro, M., Arnold, L.J., Parés, J.M., Sala, R., 2015. Extended-range luminescence chronologies suggest potentially complex bone accumulation histories at the Early-to-Middle Pleistocene palaeontological site of Huéscar-1 (Guadix-Baza basin, Spain). Quat. Int. 389, 191–212.

Demuro, M., Arnold, L.J., Aranburu, A., Sala, N., Arsuaga, J.L., 2019a. New bracketing luminescence ages constrain the Sima de los Huesos hominin fossils (Atapuerca, Spain) to MIS 12. J. Hum. Evol. 131, 76–95.

Demuro, M., Arnold, L.J., Aranburu, A., Gómez-Olivencia, A., Arsuaga, J.L., 2019b. Single-grain OSL dating of the Middle Palaeolithic site of Galería de las Estatuas, Atapuerca (Burgos, Spain). Quat. Geochronol. 49, 254–261.

Demuro, M., Arnold, L.J., Duval, M., Méndez-Quintas, E., Santonja, M., Pérez-González, A., 2020. Refining the chronology of Acheulean deposits at Porto Maior in the River Miño basin (Galicia, Spain) using a comparative luminescence and ESR dating approach. Quat. Int. 556, 96–112.

Duval, M., Arnold, L.J., Demuro, M., Parés, J.M., Campaña, I., Carbonell, E., Bermúdez de Castro, J.M., 2022. New chronological constraints for the lowermost stratigraphic unit of Atapuerca Gran Dolina (Burgos, N Spain). Quat. Geochronol., 101292 https://doi.org/10.1016/j.quageo.2022.101292.

Duval, M., Grün, R., Parés, J.M., Martín-Francés, L., Campaña, I., Rosell, J., Shao, Q., Arsuaga, J.L., Carbonell, E., Bermúdez de Castro, J.M., 2018. The first direct ESR dating of a hominin tooth from Atapuerca Gran Dolina TD-6 (Spain) supports the antiquity of Homo antecessor. Quat. Geochronol. 47, 120–137.

Duval, M., Voinchet, P., Arnold, L.J., Parés, J.M., Minnella, W., Guilarte, V., Demuro, M., Falguères, C., Bahain, J.-J., Despriée, J., 2020. A multi-technique dating study of two Lower Palaeolithic sites from the Cher valley (Middle Loire Catchment, France). Lunery-la Terre-des-Sablons Brinay-la Noira Quat. Int. 556, 79–95.

Edwards, R.L., Chen, J.H., Wasserburg, G.J., 1987. ^{238}U, ^{234}U, ^{230}Th, ^{232}Th systematics and the precise measurement of time over the past 500,000 years. Earth Planet Sci. Lett. 81, 175–192.

Falguères, C., Bahain, J.J., Yokoyama, Y., Arsuaga, J.L., Bermúdez de Castro, J.M., Carbonell, E., Bischoff, J.L., Dolo, J.M., 1999. Earliest humans in Europe: the age of TD6 gran Dolina, Atapuerca, Spain. J. Hum. Evol. 33, 343–352.

Falguères, C., Bahain, J.-J., Bischoff, J.L., Pérez-González, A., Ortega, A.I., Ollé, A., Quiles, A., Ghaleb, B., Moreno, D., Dolo, J.-M., Shao, Q., Vallverdú, J., Carbonell, E., Bermúdez de Castro, J.M., Arsuaga, J.L., 2013. Combined ESR/U-series chronology of Acheulian hominid-bearing layers at Trinchera Galería site, Atapuerca, Spain. J. Hum. Evol. 65, 168–184.

Galbraith, R.F., Roberts, R.G., Laslett, G.M., Yoshida, H., Olley, J.M., 1999. Optical dating of single and multiple grains of quartz from Jinmium rock shelter, northern Australia: Part I, experimental design and statistical models. Archaeometry 41, 339–364.

García, N., Arsuaga, J.L., Torres, T., 1997. The carnivore remains from the Sima de los Huesos Middle Pleistocene site (Sierra de Atapuerca, Spain). J. Hum. Evol. 33, 155–174.

García García, N., Feranec, R.S., Arsuaga, J.L., Bermúdez de Castro, J.M., Carbonell, E., 2009. Isotopic analysis of the ecology of herbivores and carnivores from the Middle Pleistocene deposits of the Sierra De Atapuerca, northern Spain. J. Archaeol. Sci. 36, 1142–1151.

García-Medrano, P., Ollé, A., Mosquera, M., Cáceres, I., Carbonell, E., 2015. The nature of technological changes: the Middle Pleistocene stone tool assemblages from Galería and Gran Dolina-subunit TD10.1 (Atapuerca, Spain). Quat. Int. 368, 92–111.

Guérin, G., Mercier, M., Adamiec, G., 2011. Dose-rate conversion factors: update. Ancient TL 29, 5–8.

Huguet, R., Vallverdú, J., Rodríguez-Álvarez, X.P., Terradillos-Bernal, M., Bargalló, A., Lombera-Hermida, A., Menéndez, L., Modesto-Mata, M., Van der Made, J., Soto, M., Blain, H.A., García, N., Cuenca-Bescós, G., Gómez-Merino, G., Pérez-Martínez, R., Expósito, I., Allué, E., Rofes, J., Burjachs, F., Canals, A., Bennàsar, M., Nuñez-Lahuerta, C., Bermúdez de Castro, J.M., Carbonell, E., 2017. Level TE9c of Sima del Elefante (Sierra de Atapuerca, Spain): a comprehensive approach. Quat. Int. 433A, 278–295.

Huntley, D.J., Lamothe, M., 2001. Ubiquity of anomalous fading in K-feldspars and the measurement and correction for it in optical dating. Can. J. Earth Sci. 38, 1093–1106.

Huntley, D.J., Baril, M.R., 1997. The K content of the K-feldspars being measured in optical dating or in thermoluminescence dating. Ancient TL 15, 11–13.

Jaffey, A.H., Flynn, K.F., Glendenin, L.E., Bentley, W.C., Essling, A.M., 1971. Precision measurement of half-lives and specific activities of ^{235}U and ^{238}U. Phys. Rev. C 4, 1889–1906.

Kars H., R., Wallinga, J., Cohen M., K., 2008. A new approach towards anomalous fading correction for feldspar IRSL dating-tests on samples in field saturation. Radiat. Meas. 43, 786–790.

Lisiecki, L.E., Raymo, M.E., 2005. A Pliocene-Pleistocene stack of 57 globally distributed benthic δ18O records. Paleoceanography 20, 1003.

López-García, J.M., Blain, H., De Marfà, R., García, A., Martinell, J., Bennàsar, M.Ll, Cuenca-Bescós, G., 2011. Small-mammals from the Middle Pleistocene layers of the Sima del Elefante (Sierra de Atapuerca, Burgos, northwestern Spain). Geol. Acta 9, 29–43.

Martín-Chivelet, J., Muñoz-García, M.B., Edwards, R.L., Turrero, M.J., Ortega, A.I., 2011. Land surface temperature changes in Northern Iberia since 4000 yr BP, based on δ^{13}C of speleothems. Global Planet. Change 77, 1–12.

Martínez-Pillado, V., Aranburu, A., Arsuaga, J.L., Ruiz-Zapata, B., Gil-García, M.J., Stoll, H., Yusta, I., Iriarte, E., Carretero, J.M., Edwards, L., Cheng, H., 2014. Upper Pleistocene and Holocene palaeoenvironmental records in Cueva Mayor karst (Atapuerca, Spain) from different proxies: speleothem crystal fabrics, palynology, and archaeology. Int. J. Speleol. 43, 1–14.

Méndez-Quintas, E., Santonja, M., Pérez-González, A., Duval, M., Demuro, M., Arnold, L. J., 2018. First evidence of an extensive Acheulean large cutting tool accumulation in Europe from Porto Maior (Galicia, Spain). Sci. Rep. 8, 3082.

Meyer, M., Arsuaga, J.L., de Filippo, C., Nagel, S., Aximu-Petri, A., Nickel, B., Martínez, I., Gracia, A., Bermúdez de Castro, J.M., Carbonell, E., Viola, B., Kelso, J., Prüfer, K., Pääbo, S., 2016. Nuclear DNA sequences from the Middle Pleistocene Sima de los Huesos hominins. Nature 531, 504–507.

Moreno, D., Falguères, C., Pérez-González, A., Voinchet, P., Ghaleb, B., Despriée, J., Bahain, J.-J., Sala, R., Carbonell, E., Bermúdez de Castro, J.M., Arsuaga, J.L., 2015. New radiometric dates on the lowest stratigraphical section (TD1 to TD6) of Gran Dolina site (Atapuerca, Spain). Quat. Geochronol. 30, 535–540.

Mosquera, M., Ollé, A., Rodríguez, X.P., 2013. From Atapuerca to Europe: tracing the earliest peopling of Europe. Quat. Int. 295, 130–137.

Murray, A., Arnold, L.J., Buylaert, J.-P., Guérin, G., Qin, J., Singhvi, A.K., Smedley, R., Thomsen, K.J., 2021. Optically stimulated luminescence dating using quartz. Nat. Rev. Methods Prim. 1, 72.

Ollé, A., Mosquera, M., Rodríquez, X.P., de Lombera-Hermida, A., García-Antón, M.D., García-Medrano, P., Peña, L., Menéndez, L., Navazo, M., Terradillos, M., Bargalló, A., Márquez, B., Sala, R., Carbonell, E., 2013. The early and middle Pleistocene technological record from Sierra de Atapuerca (Burgos, Spain). Quat. Int. 295, 138–167.

Ollé, A., Mosquera, M., Rodríquez-Alvarez, X.P., García-Medrano, P., Barsky, D., de Lombera-Hermida, A., Carbonell, E., 2016. The Acheulean from Atapuerca: three steps forward, one step back. Quat. Int. 411, 316–328.

Ortega, A.I., Campaña, I., Benito-Calvo, A., Parés, J.M., Pérez-González, A., Martín-Merino, M.A., Huguet, R., Vallverdú, J., Pérez, R., Aramburu, A., Arsuaga, J.L., Bermúdez de Castro, J.M., Carbonell, E., 2013a. Galería Baja y su relación con el yacimiento de la Sima del Elefante (Cueva Mayor, Sierra de Atapuerca, Burgos). VIII Reunión de Cuaternario Ibérico, Sevilla, pp. 87–90.

Ortega, A.I., Benito-Calvo, A., Pérez-González, A., Martín-Merino, M.A., Pérez-Martínez, R., Pares, J.M., Aramburu, A., Arsuaga, J.L., Bermúdez de Castro, J.L., Carbonell, E., 2013b. Evolution of multilevel caves in the Sierra de Atapuerca (Burgos, Spain) and its relation to human occupation. Geomorphology 196, 122–137.

Pacher, M., Stuart, A.J., 2009. Extinction chronology and palaeobiology of the cave bear (*Ursus spelaeus*). Boreas 38, 189–206.

Parés, J.M., Pérez-González, A., Rosas, A., Benito, A., Bermúdez de Castro, J.M., Carbonell, E., Huguet, R., 2006. Matuyama-age lithic tools from the Sima del Elefante site, Atapuerca (northern Spain). J. Hum. Evol. 50, 163–169.

Parés, J.M., Arnold, L., Duval, M., Demuro, M., Pérez-González, A., Bermúdez de Castro, J.M., Carbonell, E., Arsuaga, J.L., 2013. Reassessing the age of Atapuerca-TD6 (Spain): new paleomagnetic results. J. Archaeol. Sci. 40, 4586–4595.

Prescott R., J., Hutton T., J., 1994. Cosmic ray contribution to dose rates for luminescence and ESR dating: large depths and long-term variations. Radiat. Meas. 23, 497–500.

Rosas, A., Huguet, R., Pérez-González, A., Carbonell, E., Bermúdez de Castro, J.M., Vallverdú, J., van der Made, J., Allué, E., García, N., Martínez-Pérez, R., Rodríguez, J., Sala, R., Saladie, P., Benito, A., Martínez-Maza, C., Bastir, M., Sánchez, A., Parés, J.M., 2006. The "Sima del Elefante" cave site at Atapuerca (Spain). Estud. Geol. 62, 327–348.

Stevens, T., Buylaert, J.-P., Murray, A.S., 2009. Towards development of a broadly-applicable SAR TT-OSL dating protocol for quartz. Radiat. Meas. 44, 639–645.

Vallverdú i Poch, J., 2017. Soil-stratigraphy in the cave entrance deposits of Middle Pleistocene age at the Trinchera del Ferrocarril sites (Sierra de Atapuerca, Spain). Quat. Int. 433, 199–210.